Croatian Society for Materials Protection

Metalurgija/Metallurgy

Vol. 65 No. 1 / 2026

Analysis of the Trafficability of Spherical Internal Detectors in Pipelines

Yue Cui[1], Hui-Qing Lan[2,*], Nan Lin[3], Ke-Xin Tan[4], Zhao-Qi Jiang[1], Xiang-Bin Yang[1]

https://doi.org/10.64486/m.65.1.10

[1] Hebei Key of Laboratory of Intelligence Equipment Digitalize Design and Process Simulation, Tangshan University, Tangshan 063000, China; (cuiyue@tsc.edu.cn, 794703392@qq.com, 603010204@163.com)
[2] Key Laboratory of Vehicle Advanced Manufacturing, Measuring and Control Technology (Ministry of Education), Beijing Jiaotong University, Beijing 100044, China;Tangshan Research Institute of Beijing Jiaotong University, Tangshan 063000, China; hqlan@bjtu.edu.cn
[3] China Special Equipment Inspection and Research Institute, Beijing 100029, China; sy_linnan@163.com
[4] China University of Petroleum (Beijing), Beijing 102249, China; 2022010937@student.cup.edu.cn
* Correspondence: hqlan@bjtu.edu.cn

Type of the Paper: Article
Received: August 20, 2025
Accepted: October 13, 2025

Abstract: This study aims to enhance the motion stability of a spherical internal detector within a flow field, thereby preventing jamming or deviations during the inspection process. Firstly, a fluid-structure interaction model of a spherical detector in a pipeline was built, and flow field calculations were performed for a straight pipe and a 60° elbow with a 600 mm diameter, examining various ball-to-pipe diameter ratios. The analysis, including the flow field and pressure distribution characteristics of the spherical internal detector within the pipe configurations, was supplemented by experimental verification. The findings reveal that the thrust generated by the spherical internal detector correlates positively with the ball-to-pipe diameter ratio. However, an excessively high ratio 0.8 led to a rapid decrease in fluid velocity in the wake region and an increase in the radial region. Significantly, when the spherical internal detector navigates through a 60° pipe elbow, its angular velocity triples compared to that in a straight pipe section, potentially reducing the detector's service life. For 600 mm diameter pipes, it is recommended that the optimal condition is achieved with a ball-to-pipe diameter ratio of 0.6 and an initial fluid flow velocity of 1.5 m/s to extend service life while ensuring optimal trafficability of the spherical internal detector.

Keywords: spherical internal detector; fluid-structure interaction; trafficability; flow velocity; angular velocity

1. Introduction

Pipelines are critical infrastructural facilities in urban environments, playing a central role in both the city's functionality and in the daily lives of its inhabitants. The economic repercussions of pipeline leaks in developing nations are substantial, with annual losses estimated to reach as high as $2.9 billion [1]. China's expansive pipeline network, now exceeding 3 million kilometers, is increasingly plagued by leakage issues. Leaks within urban water supply networks not only result in significant water wastage but also pose grave safety risks. Presently,

over 66 % of pipelines in operation in China have been in use for more than two decades, underscoring the urgency of effective leakage detection [2, 3]. The development and deployment of in-pipe inspection robots have emerged as a focal area of research, drawing attention due to their capacity for omnidirectional movement, minimal flow resistance, and ability to navigate through complex pipeline systems [4, 5].

In the domain of in-service pipeline inspection, notable advancements include the hinged-structure robot designed by Choi et al. [6], which is propelled by motors located at both ends; the spiral spring-equipped mobile robot by Kurata et al. [7] for navigating entangled flexible pipes of small diameters; and the motion planning algorithm for a caterpillar-type robot by Kwon et al. [8], suitable for pipes with diameters between 80 and 100 mm. Chan et al. [9] proposed a portable and automatic robot which exhibited superior capacities in complicated pipe environments for turning into 90° elbows, that can be applied to any pipeline system.

The innovative 'smartball' developed by Pure Technology Company in Canada, which employs acoustic sensors to detect pipeline leaks, represents a significant proprietary advancement in the field [10]. Similarly, Tianjin University has developed a spherical internal detector prototype and introduced a micro-leak detection strategy utilizing this technology, which has seen initial application in water supply pipeline projects [11, 12]. Huang Xin-jing et al. has developed a spherical internal detector prototype and introduced a micro-leak detection strategy utilizing this technology, which has seen initial application in water supply pipeline projects [13]. Additionally, Wang et al. [14] have developed a methodology for measuring pipeline inclination through experiments conducted with an in-pipe spherical detector (SD) in steel pipes; Huang et al. [15] achieved an absolute localization error of 1.2 km in pipeline mapping using a mobile spherical detector with 3D rotational capabilities. Lastly, Xu [16] introduced a pipeline leak identification method employing a spherical detector, which combines variational mode decomposition for enhanced accuracy.

Extensive research has been undertaken on pipeline inspection detectors; however, optimizing the motion stability of these passive devices within fluid flows, preventing their entrapment or deviation under complex flow conditions, ensuring their navigability, and prolonging their operational lifespan continue to constitute principal research objectives. This study analyzed the dynamic characteristics of the flow field across various diameters and the angular velocity and acceleration of the detector under different initial velocities during collisions, leading to a deeper understanding of the thrust characteristics associated with this detector.

2. Theoretical Model

When a spherical internal detector navigates through a pipeline, the fluid medium is assumed to be incompressible, and the large eddy simulation technique is employed. The flow adheres to the fundamental equations of fluid mechanics, with thermal exchanges between the internal and external environments of the pipeline being disregarded. The time-averaged control equation derived from the three-dimensional Navier-Stokes equations is presented as follows [17, 18]:

$$\frac{\partial \rho}{\partial t}+\frac{\partial}{\partial x_i}\left(\rho u_i\right)=0 \tag{1}$$

where, u_i denotes the velocity components along the x, y, and z axes, and ρ indicates the fluid's density.
Momentum equations:

$$\frac{\partial}{\partial t}\left(\rho u_i\right)+\frac{\partial}{\partial x_j}\left(\rho u_i u_j\right)=-\frac{\partial p}{\partial x_i}+\frac{\partial}{\partial x_j}\left[\mu\left[\frac{\partial u_i}{\partial x_j}+\frac{\partial u_j}{\partial x_i}-\frac{2}{3}\delta_{ij}\frac{\partial u_i}{\partial x_i}\right]\right]+\frac{\partial}{\partial x_j}\left(-\overline{\rho u_i u_j}\right) \tag{2}$$

In Equation (2), P represents the pressure exerted on each infinitesimal fluid element within the pipeline, while $\overline{\rho u_i u_j}$ is the Reynolds stress tensor, further elaborated in Equation (3):

$$\overline{\rho u_i u_j}=\mu_t\left(\frac{\partial u_i}{\partial x_j}+\frac{\partial u_j}{\partial x_i}\right)-\frac{2}{3}\rho k\delta_{ij} \tag{3}$$

https://doi.org/10.64486/m.65.1.10

where, δ_{ij} is the Kronecker delta, and μ_t represents the eddy viscosity:

$$\mu_t = \rho \frac{k}{\omega} \tag{4}$$

The variables k and ω signify the turbulent kinetic energy and its dissipation rate, respectively. These are calculated using Equations (5) and (6):

$$\frac{\partial(\rho k)}{\partial t} + \frac{\partial(\rho k u_i)}{\partial x_i} = \frac{\partial}{\partial x_j}\left(\Gamma_k \frac{\partial k}{\partial x_j}\right) + G_k - Y \tag{5}$$

$$\frac{\partial(\rho \omega)}{\partial t} + \frac{\partial(\rho \omega u_i)}{\partial x_i} = \frac{\partial}{\partial x_j}\left[\Gamma_\omega \frac{\partial \omega}{\partial x_j}\right] + G_\omega - Y_\omega \tag{6}$$

In Equations (5) and (6), G_k denotes the generation of turbulent kinetic energy due to the mean velocity gradient. G_ω is a coefficient dependent on ω. Γ_ω and Γ_k are the effective diffusivities for k and ω, respectively, while Y_k and Y_ω represent the dissipation of k and ω due to turbulence.

When the spherical internal detector moves along with the fluid in the pipeline, the magnitude of thrust it experiences is influenced by the fluid velocity. The relationship governing this thrust is formulated in Equation (7):

$$F_t = \left(\frac{\pi d^2}{4}\right)\left(\frac{1}{2}\rho V^2\right) C_D \tag{7}$$

where, D stands for the pipeline diameter, d is the diameter of the spherical internal detector, and C_D denotes the thrust coefficient.

By discretizing the overall structure of the pipeline using the finite element method, the dynamic equation governing the pipeline can be expressed as follows [19]:

$$\boldsymbol{M}\ddot{x} + \boldsymbol{C}\dot{x} + \boldsymbol{K}\boldsymbol{X} = F(t) \tag{8}$$

where, $\boldsymbol{M}$ represents the mass matrix; $\boldsymbol{C}$ is the damping matrix; $\boldsymbol{K}$ denotes the stiffness matrix; $\boldsymbol{X}$ is the displacement vector, and $F(t)$ is the load induced by fluid motion.

3. Flow Field and Collision Analysis

A spherical internal detector is selected with diameters ranging from 240 mm to 480 mm, and a fluid-structure interaction model is developed for a pipe with a diameter of 600 mm. Let r denote the ratio of the spherical internal detector's diameter to the pipe diameter. The pipe's interior is classified as a fluid region, utilizing water as the conveying medium. The flow field calculation domain's left boundary is configured as a velocity inlet with conditions ranging from 0.5 m/s to 2.5 m/s, while the right boundary is set as a pressure outlet. The pipeline's inner surface, in contact with the fluid, adheres to a no-slip wall condition. The staggered method is employed for numerical solutions, and tetrahedral mesh generation is depicted in Figure 1a.

https://doi.org/10.64486/m.65.1.10

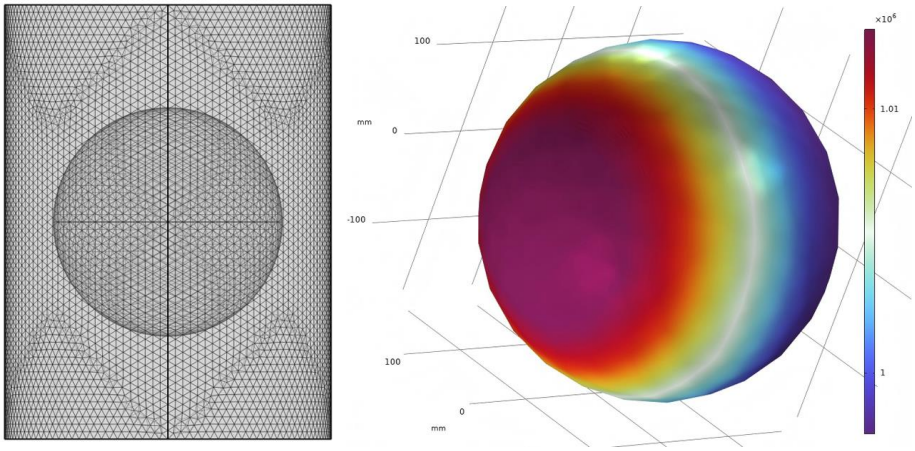

a) Grid division b) Surface pressure distribution / Pa

Figure 1. Grid division and surface pressure distribution of the spherical internal detector

Figure 1 b) illustrates the pressure distribution on the spherical internal detector's surface, influenced by fluid propulsion at a flow velocity of 1.5 m/s and a detector diameter of 360 mm. The pressure distribution is markedly non-uniform along the flow direction; the upstream face exhibits a high-pressure area due to fluid stagnation, whereas the downstream face experiences a low-pressure area as a result of flow separation. This pressure differential across the detector generates a thrust force acting on it.

A pipeline model with a 600 mm diameter and a 1600 mm length was established to simulate five conditions (r = 0.4, 0.5, 0.6, 0.7, 0.8) at an initial flow velocity of 1.5 m/s.

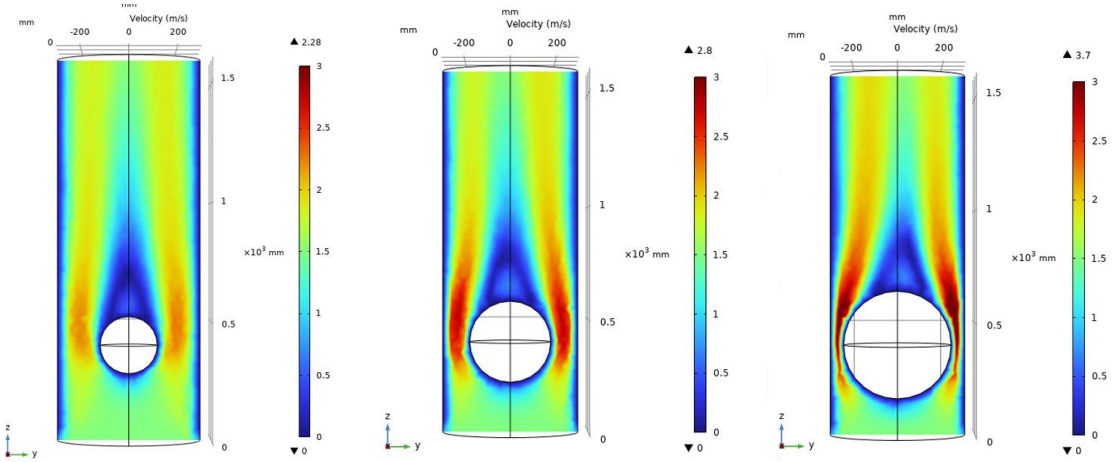

a) r = 0.4 b) r = 0.6 c) r = 0.8

Figure 2. Velocity contour plot around the spherical internal detector in the YZ plane (m/s)

In Figure 2, as the fluid propels the spherical internal detector, the flow velocity in the wake region decreases due to viscous effects. As r increases, the area of this low-velocity wake region correspondingly expands. Concurrently, the fluid velocity in the radial region around the spherical internal detector along the pipeline evidences a significant increase, ranging from 2.1 m/s at r = 0.4 to 3.7 m/s at r = 0.8. These velocity variations in different regions potentially contribute to an increase in the angular velocity during collisions between the spherical internal detector and the pipe.

The fluid velocity along the pipe axis at the edge of the spherical internal detector, derived for different diameters, is shown in Figure 3.

https://doi.org/10.64486/m.65.1.10

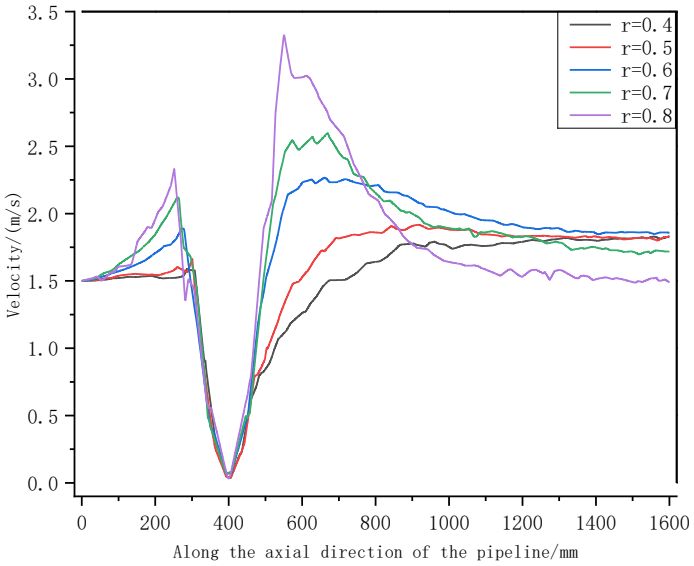

Figure 3. Velocity at the edge of the spherical internal detector along the pipeline axis

As the diameter of the spherical internal detector was increased from 240 mm to 480 mm, a notable rise was observed in the maximum fluid velocity at the edge of the detector along the pipeline axis, escalating from 2.1 m/s to 3.4 m/s. Concurrently, the velocity variation pattern in the wake region behind the detector became more pronounced. Specifically, at a radial distance r = 0.4, the fluid velocity stabilized at 1.8 m/s; however, at r = 0.8, the velocity rapidly decreased from 3.4 m/s to 1.5 m/s, posing a risk of causing the detector to roll and collide. The pressure variations at the edge of the detector are depicted in Figure 4.

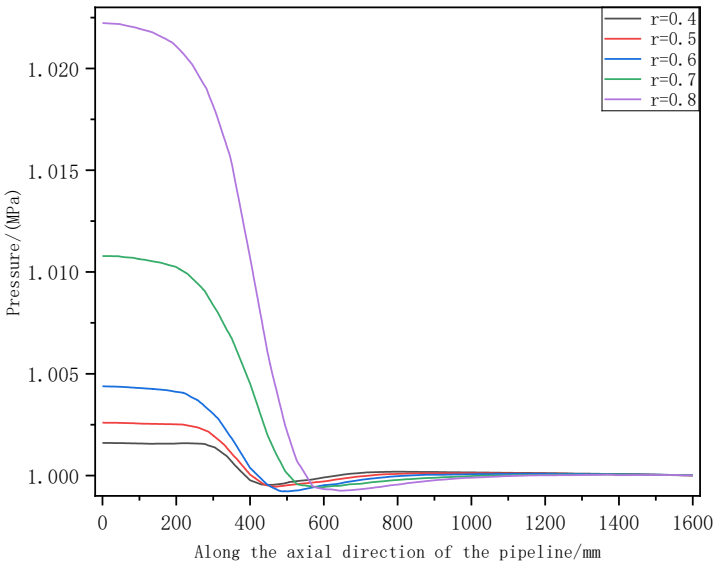

Figure 4. Pressure at the edge of the spherical internal detector along the pipeline

With the increase in the diameter of the spherical internal detector from 240 mm to 480 mm, the maximum pressure differential in the pipeline surged from 2 kPa to 22 kPa. Although the heightened pressure differential could provide greater thrust to the detector, the increased diameter also elevated the risk of obstruction in areas with flow alterations, such as elbows and T-junctions.

https://doi.org/10.64486/m.65.1.10

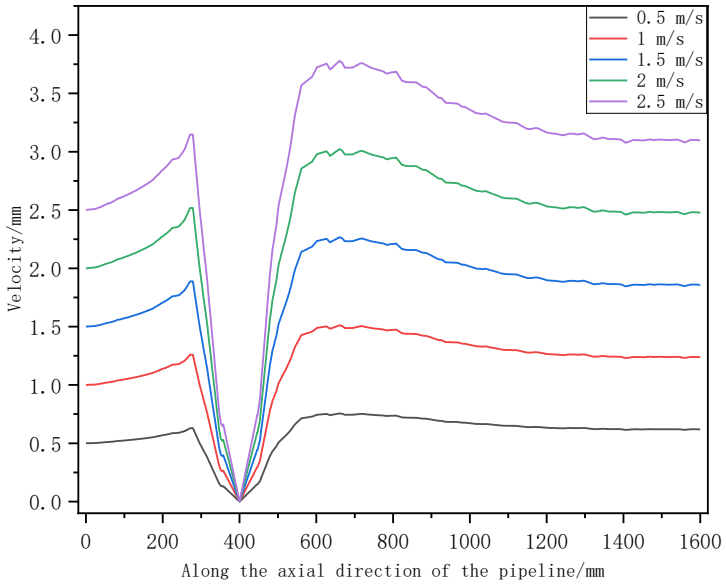

a) Velocity variation / (m/s)

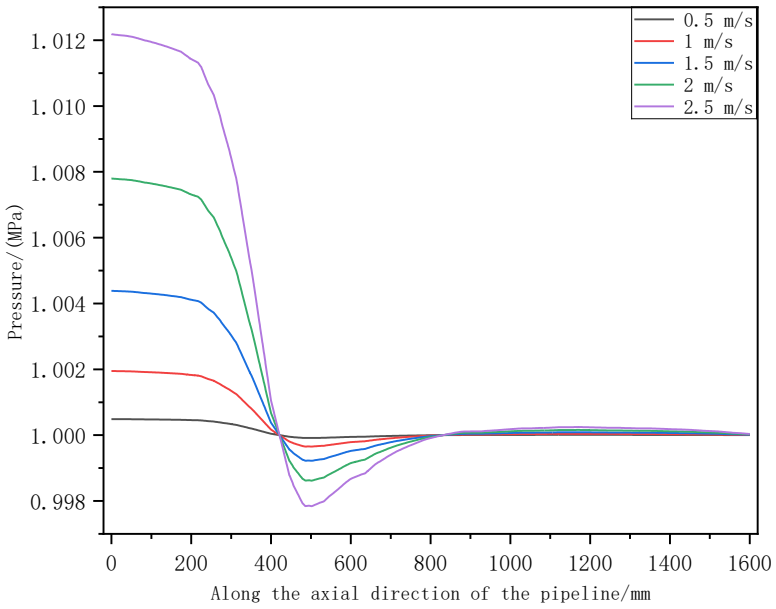

b) Pressure variation / MPa

Figure 5. Velocity and pressure at the edge of the spherical internal detector under varying flow velocities along the pipe line

As the initial flow velocity was elevated from 0.5 m/s to 2.5 m/s (Figure 5 a)), the maximum fluid velocity at the edge of the spherical internal detector rose from 0.7 m/s to 3.8 m/s along the pipeline axis. Meanwhile, the velocity variation trend in the wake region of the detector remained smooth. Alongside this, the maximum pressure differential increased from 1 kPa to 14 kPa along the pipeline axis (Figure 5 b)). It was observed that

https://doi.org/10.64486/m.65.1.10

an increase in initial flow velocity exerted a less pronounced effect on the pressure differential of the detector compared to the effect of an increase in its diameter.

A test platform with a 600 mm diameter pipeline, constructed from polycarbonate material, was equipped with a variable frequency water pump to maintain a flow rate of 1.5 m/s for testing the passage of a spherical internal detector with a diameter of 360 mm. A high-speed camera was employed to capture the flow velocities of the detector, with the experimental setup including a detector input and recovery port as illustrated in Figure 6.

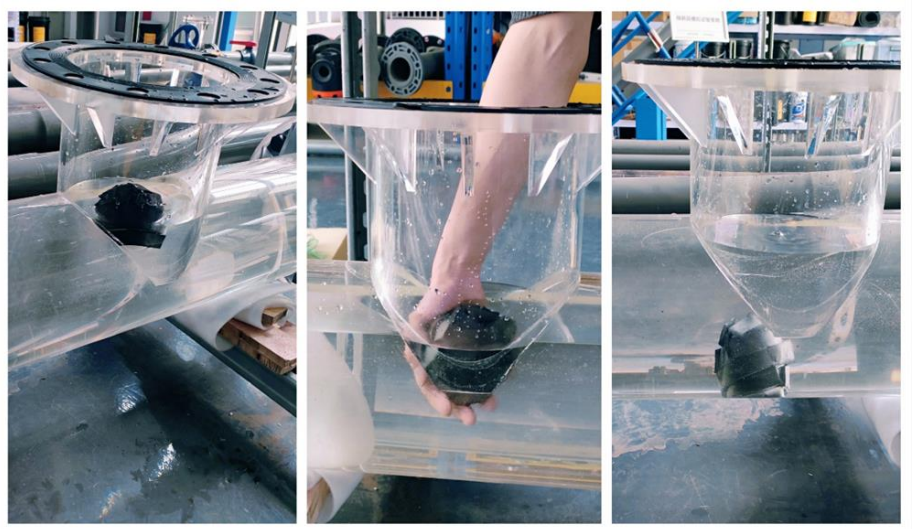

Figure 6. Spherical internal detector input into the pipeline testing platform

The axial velocity of the spherical internal detector along the pipeline was recorded at an initial flow rate of 1.5 m/s. The data collection points, spaced 300 mm apart, were analyzed and compared with simulated data as shown in Figure 7.

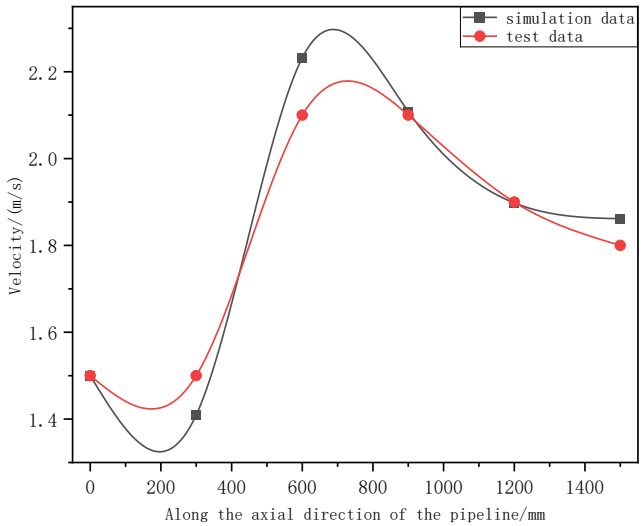

Figure 7. Simulation and experimental data comparison of the velocity of the detector

The spherical internal detector was in a state of acceleration upon deployment, achieving a peak speed of 2.1 m/s in the experiment before gradually returning to the initial flow velocity. The maximum discrepancy

https://doi.org/10.64486/m.65.1.10

observed between the experimental and simulated data was 6.4 %, substantiating the viability of the simulation model. The simulation depicting the flow field within 60° climbing section of an elbow is illustrated in Figure 8.

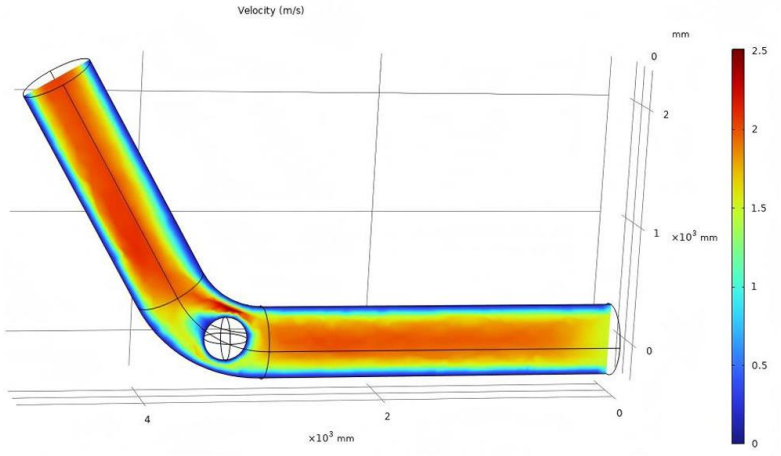

Figure 8. Velocity of the spherical internal detector along the YZ plane within the 60° climbing pipe

As the spherical internal detector traversed a 360 mm section through a 60° elbow, as shown in Figure 8, it reached a maximum velocity of 2.5 m/s due to changes in the flow field. This resulted in a velocity differential of 1 m/s between the inner and outer sides of the elbow, thereby enhancing the rotational tendency of the detector.

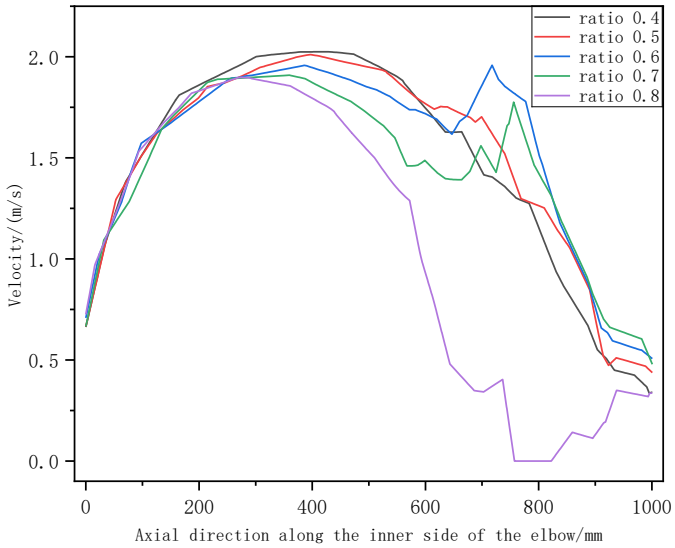

Figure 9. Velocity profile along the tangent at the inner side of the elbow for the spherical internal detector under varying *r* values

Figure 9. presents the velocity profiles extracted along the tangent to the spherical internal detector at the inner side of the 60° elbow. As the detector's diameter increased from 240 mm to 480 mm, the maximum fluid velocity decreased from 2 m/s to 1.8 m/s. For diameters less than 420 mm ($r < 0.7$), the decrease in fluid velocity was consistent. However, at a diameter of 480 mm ($r = 0.8$), the minimum fluid velocity at the inner side of the elbow approached zero, increasing the likelihood of the detector becoming jammed.

When operational within pipelines, the spherical internal detector inevitably contacts and collides with the inner walls. These collisions alter the detector's orientation and motion dynamics. Virtual prototyping technology was employed to simulate collision dynamics for a detector with a diameter of 360 mm.

https://doi.org/10.64486/m.65.1.10

The resulting dynamic simulations of the detector's angular velocity for varying initial flow velocities are depicted in Figure 10.

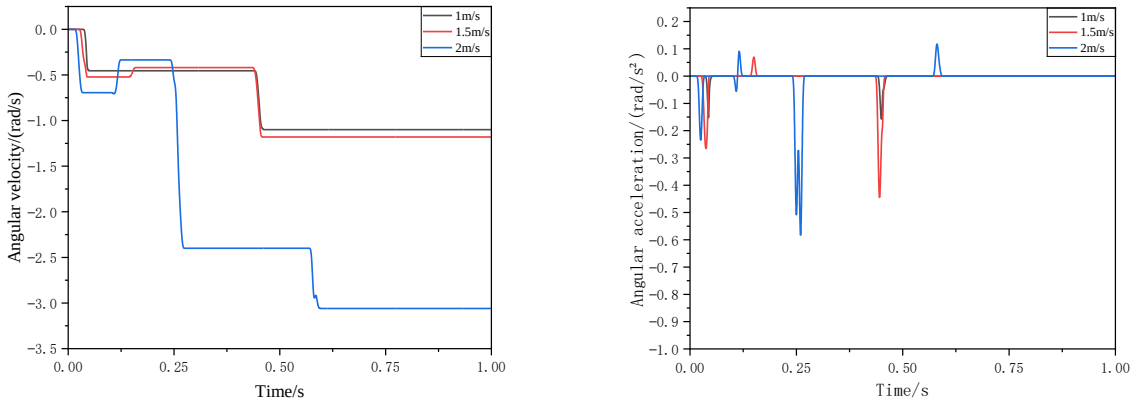

a) Angular velocity variation (rad/s) **b**) Angular acceleration variation (rad/s²)

Figure 10. Analysis of angular velocity and angular acceleration of the detector at different initial flow velocities

In Figure 10, an increase in the initial flow velocity led to a corresponding increase in ball collision frequency. At a flow velocity of 1 m/s, the detector's maximum angular velocity during collision reached 1.1 rad/s, and its maximum angular acceleration was 0.15 rad/s². When the flow velocity increased to 2 m/s, the maximum angular velocity escalated to 3 rad/s, and the angular acceleration peaked at 0.58 rad/s². Merely increasing the initial flow velocity to enhance the navigability of the detector could consequently reduce its service life. The impact within a 60° elbow with a diameter of 600 mm is depicted in Figure 11.

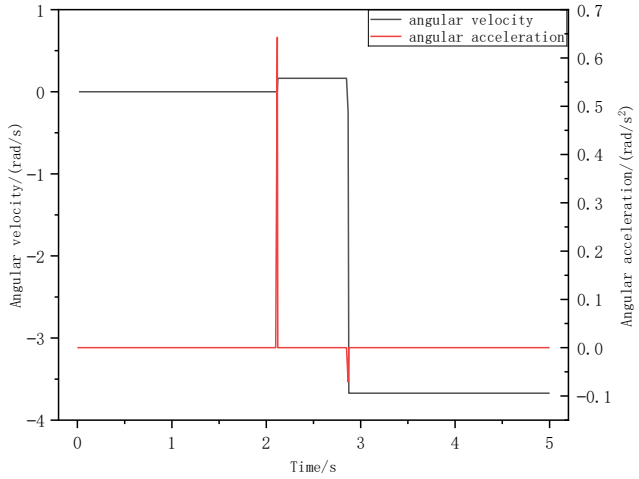

Figure 11. Analysis of angular velocity and acceleration of the spherical internal detector within the 60° elbow

As illustrated in Figure 11, when the 360 mm spherical internal detector navigated through a 60° elbow at an initial flow velocity of 1.5 m/s, the collision induced a maximum angular velocity of 3.6 rad/s and a maximum angular acceleration of 0.65 rad/s². Notably, when the detector traversed the 60° elbow at the same initial flow velocity of 1.5 m/s, the intensity of the collision was greater than that experienced in a straight section of the pipe.

https://doi.org/10.64486/m.65.1.10

4. Conclusions

This study analyzed the flow field dynamics of a spherical internal detector across various diameters, leading to a deeper understanding of the thrust characteristics associated with this detector. The accuracy of the simulation model was confirmed by integrating experimental velocity measurements. Dynamic analyses were conducted to calculate the angular velocity and acceleration of the detector under different initial velocities during collisions. The findings are summarized as follows:

The thrust exerted by the spherical internal detector demonstrated a positive correlation with the ratio of the ball-to-pipe diameter *r*. Notably, at an excessively high ratio (r = 0.8), the flow velocity in the wake region of the detector sharply decreased from 3.4 m/s to 1.5 m/s. This significant reduction in flow velocity was likely to induce rolling and collision of the detector. Conversely, when the ratio increased, the fluid velocity around the detector markedly rose from 2.1 m/s (r = 0.4) to 3.7 m/s (r = 0.8). These variations in radial velocity could lead to increased angular acceleration during collisions.

The increase in initial flow velocity had a less pronounced effect on the thrust of the detector compared to the diameter ratio r. Furthermore, higher flow velocities (2.5 m/s) tended to induce turbulence and instability within the flow field, which in turn affected the pose and motion pattern of the spherical internal detector.

At an initial flow velocity of 1.5 m/s, the spherical internal detector reached its maximum angular velocity (1.2 rad/s) and acceleration (0.45 rad/s²) within a straight pipeline. When navigating through a 60° elbow, the maximum angular velocity and acceleration escalated to 3.6 rad/s and 0.65 rad/s², respectively. Structural changes in the flow channel intensified collisions between the detector and the pipeline's inner wall. Simply increasing the initial flow rate to improve navigability could potentially reduce the service life of the detector.

The current research was limited to analyzing the trafficability of spherical internal detectors in 60° elbows under the condition that the water was the transport medium in the pipeline. In subsequent work, multiple rounds of experiments will be conducted to validate the performance of the spherical internal detector (r = 0.6) in 90° elbow and T-junction configurations under the condition that gas is the transport medium. These studies will focus on optimizing the dynamic motion characteristics of the detector while ensuring its navigability and extending its operational lifespan.

Acknowledgments: This research was funded by Xiong'an New Area Science and Technology Innovation Project, National Key R&D Program of China (no. 2022XAGG0147); and the Development Funds of the Central Government for Local Science and Technology (no. 236Z1701G).

References

[1] T. T. Zhong, D. H. Li, F. X. Li., "Research Progress on Corrosion Behavior of Oil and Gas Pipelines" *Corrosion and Protection*, vol. 41, no. 5, pp. 81–89, Sep. 2025, (in Chinese), https://doi.org/10.11973/fsyfh230188

[2] F. S. Jiang, Z.Q. Xie, J. R. Xu et al. "Informatization Countermeasures of China's Underground Pipeline Accidents Under the Background of Urbanization," *Urban Geotechnical Investigation & Surveying*, vol. 5, pp.161-165,2023, (in Chinese)

[3] W. W. Zhang, R. K. Lu, J. Z. Chen et al. "Centerline mapping technology of small diameter oil and gas pipeline based on MEMS inertial navigation system", Nondestructive Testing, vol. 45, no. 07, pp. 41-44+52, 2023, https://doi.org/10.11973/wsjc202307009

[4] P. C. Chen, Y. B. Ma, B.Z. Zhang et al. "Construction and Development of Modern Pipeline Transportation System," *Science and Technology Foresight*, vol. 3, no. 02, pp. 8-18, 2024, https://doi.org/10.3981/j.issn.2097-0781.2024.02.001

[5] Y. F. Wu, G.N. Shi, B. Guo et al. "Analysis of Several Scene Application of Oil and Gas Pipeline In-line Inspection Technology," China Special Equipment Safety, vol.10, no. 10, pp.41-45+55, 2024, (in Chinese)

[6] [6] H.R. Choi, S.M. Ryew. "Robotic system with active steering capability for internal inspection of urban gas pipelines," *Mechatronics*, vol. 32, no. 5, pp. 713-736, 2022, https://doi.org/10.1016/S0957-4158(01)00022-8

https://doi.org/10.64486/m.65.1.10

[7] M Kurata, T Takayama, T Omata. "*Helical rotation in-pipe mobile robot*", in 3rd IEEE RAS & EMBS Int. Cof. on Biomedical Robotics and Biomechatronics, Tokyo, Japan, 2020, pp. 313-318, https://doi.org/10.1109/BIOROB.2010.5628009

[8] Y.S. Kwon, B.J. Yi. "Design and motion planning of a two module collaborative indoor pipeline inspection robot," *IEEE Transactions on Robotics*, vol. 28, no. 3, pp. 681-696, 2012, https://doi.org/10.1109/TRO.2012.2183049

[9] C. P. Y. Chan, Z. J. Qu, K. H. Shiu et al. "In-Pipe Maintenance Robot Using Spray-In-Place Pipe Technique for Long-Distance and Complex Pipe Environment,". *Journal of Field Robotics*, vol. 42, no. 4, pp. 1226-1243, 2025, https://doi.org/10.1002/rob.22440

[10] Y. Tian, R. Y. XU. "A review of the structural design of the deformation mechanism of spherical mobile robots," *Modern Manufacturing Engineering*, vol. 7, pp. 139-148, 2025 (in Chinese).

[11] T. S. Xu. "*Research on Detection Technologies of Small Leakage in Liquid Pipeline Based on Spherical Inner Detector*," Ph.D. dissertation, School of Precision Instrument and Opto-Electronics Engineering，Tianjin University, China, 2023. (in Chinese).

[12] L. Wang. "*Study on internal detection and localization of small leak in water supply pipelines*," M.S. thesis, School of Precision Instrument and Opto-Electronics Engineering，Tianjin University, China, 2023. (in Chinese).

[13] X.J. Huang, Y.P. Yan, L.J. Pei et al. "Leak location method of heated water pipeline networkbased on shortest path planning," *Chinese Journal of Scientific Instrument*, vol. 44, no. 8, pp. 164-172, 2023, [Online]. Available: https://www.sciengine.com/CJSI/articleIndex?doi=10.19650/j.cnki.cjsi.2210524&scroll=

[14] Y. Wang, J.L. Wang, J.Y. Ma, et al. "Subsea pipeline spanning detection using a spherical detector with AC magnetic proximity switches," *Measurement*, vol. 244, no. 28, pp. 116475, 2025, https://doi.org/10.1016/j.measurement.2024.116475

[15] X. Huang, S. Chen, S. Guo, et al. "A 3D Localization Approach for Subsea Pipelines Using a Spherical Detector," *IEEE Sensors Journal*, vol. 17, no. 6, pp. 1828-1836, https://doi.org/10.1109/JSEN.2016.2586998

[16] T. S. Xu, Z. M. Zeng, X. J. Huang et al. "Pipeline leak detection based on variational mode decomposition and support vector machine using an interior spherical detector," *Process Safety and Environmental Protection*, vol. 153, pp. 167-177, 2021, https://doi.org/10.1016/j.psep.2021.07.024

[17] C. Boe, J. Rodriguez, C Plazaola et al. "A Hydrodynamic Assessment of a Remotely Operated Underwater Vehicle Based on Computational Fluid Dynamic: Part 1 numerical simulation," *CMES Computer Modeling in Engineering & Sciences*, vol. 90, no. 2, pp. 165-177, 2013, https://doi.org/10.3970/cmes.2013.090.165

[18] Z. W. Huang, B. W. Zhang, M. Z. Tang et al. "Unity of basic equations of elasticity and fluid mechanics," *Mechanics in Engineering*, vol. 44, no. 03, pp. 672-676, 2022, https://doi.org 10.6052/1000-0879-21-534

[19] Z. H. Liu, D. D. Hou, B. J. Lu et al. "Research on fluid-solid boundary feature learning network in fluid-solid simulation," *Ship Science and Technology*, 2025, (in Chinese).

https://doi.org/10.64486/m.65.1.10